Cell Reports

Article

G-Protein-Coupled Receptor SRBC-48 Protects against Dendrite Degeneration and Reduced Longevity Due to Infection

Graphical Abstract

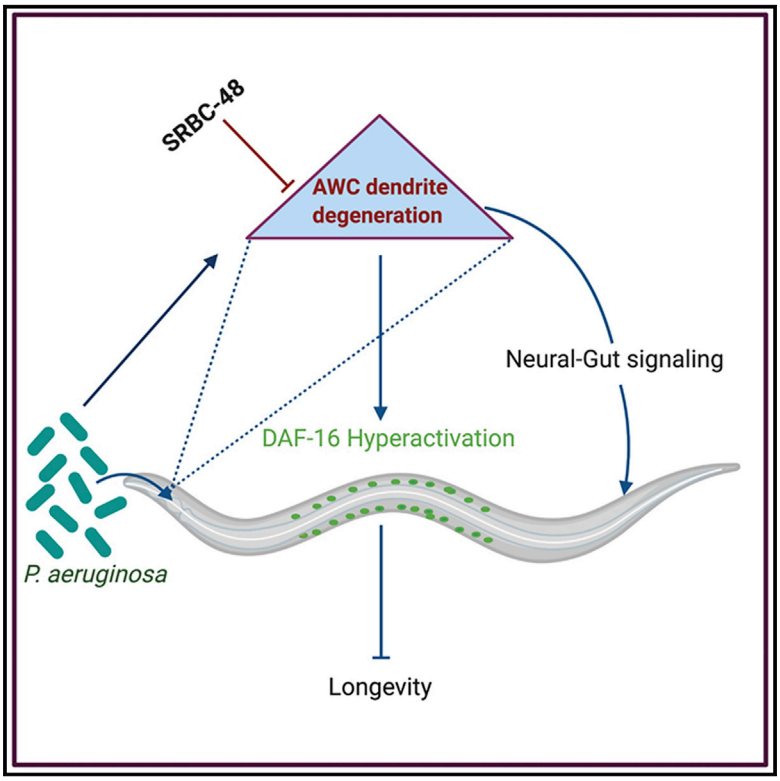

Authors

Supender Kaur, Alejandro Aballay

Correspondence

aballay@ohsu.edu

In Brief

Kaur and Aballay show that the G-protein-coupled receptor SRBC-48 functions cell autonomously in AWC neurons to protect from dendrite degeneration caused by infection with *Pseudomonas aeruginosa*. Dendrite degeneration in AWC results in decreased longevity that may be due, in part, to hyperactivation of the FOXO family transcription factor DAF-16.

Highlights

- SRBC-48 is a GPCR that protects *C. elegans* against *P. aeruginosa*-induced degeneration
- SRBC-48 functions in AWC neurons to protect against dendrite degeneration
- Dendrite degeneration hyperactivates DAF-16 in *srbc-48* animals and decreases longevity
- DAF-16 inhibition rescues the reduced lifespan caused by degeneration in *srbc-48* animals

Kaur & Aballay, 2020, Cell Reports *31*, 107662
May 19, 2020
https://doi.org/10.1016/j.celrep.2020.107662

CellPress

Cell Reports

CellPress
OPEN ACCESS

Article

G-Protein-Coupled Receptor SRBC-48 Protects against Dendrite Degeneration and Reduced Longevity Due to Infection

Supender Kaur[1] and Alejandro Aballay[1,2,*]
[1]Department of Molecular Microbiology and Immunology, Oregon Health & Science University, Portland, OR 97239, USA
[2]Lead Contact
*Correspondence: aballay@ohsu.edu
https://doi.org/10.1016/j.celrep.2020.107662

SUMMARY

Increasing evidence suggests that deficient immune modulation and microbial infections underline neurodegeneration, but the mechanisms remain obscure. Here, we show that the G-protein-coupled receptor (GPCR) SRBC-48, which belongs to the class BC serpentine receptors, has a protective role in *Caenorhabditis elegans* dendrite degeneration caused by *Pseudomonas aeruginosa* infection. Our results indicate that SRBC-48 functions in a cell-autonomous manner in AWC neurons to protect against infection-associated dendrite degeneration. The absence of SRBC-48 results in a reduced lifespan caused by a pathogen infection early in life that induces dendrite degeneration. The decreased longevity in animals deficient in SRBC-48 is due to uncontrolled activation of immune genes, particularly those regulated by the FOXO family transcription factor DAF-16 that is part of the insulin/insulin-like growth factor (IGF)-1 receptor homolog DAF-2. These results reveal how an infection early in life can not only induce dendrite degeneration but also reduce lifespan.

INTRODUCTION

Neurodegenerative diseases are important medical problems characterized by the progressive degeneration or death of one or more types of neurons. Dendrites, the primary site for entry of neural signals into neurons, have been reported to get degenerated in various pathological conditions including neurodegenerative and cognitive disorders (Kweon et al., 2017; Kwon et al., 2018). Recent evidence indicates that degeneration involves not only cell-autonomous processes but also cell-non-autonomous mechanisms. The role of activated microglia in disease progression in various degenerative neurological conditions (Heneka et al., 2014) points toward the involvement of cell-non-autonomous factors. Increasing evidence suggests that immune modulators play a role in different neurodegenerative diseases, including Alzheimer's and multiple sclerosis (Camara-Lemarroy et al., 2018; Cao and Zheng, 2018). The gut microbiome and pathogenic microbes like herpes simplex virus-1, human immunodeficiency virus (HIV), and hepatitis C virus (HCV) have been identified as potential candidates that play a role in Alzheimer's disease (AD) (Cho and Blaser, 2012; Hill et al., 2014; Huang et al., 2014; Mancuso et al., 2014; Miklossy, 2011; Poole et al., 2017). Additionally, microbial infections have also been also linked to several of the changes seen in AD patients, like cognitive deficits, inflammation, brain cell atrophy, and altered gene expression (Heintz and Mair, 2014; Kim et al., 2013; Yatsunenko et al., 2012).

The nematode *Caenorhabditis elegans* has been extensively used to study age-associated neurodegeneration because of the simplicity of its nervous system and the mapping of its entire connectome, which make it easy to use as a model for neuroscience studies (Cook et al., 2019). Moreover, it was found that exposure to *Streptomyces venezuelae* caused dopaminergic neurodegeneration (Caldwell et al., 2009) and that exposure to *Pseudomonas aeruginosa* triggered changes in neural dendrites that are hallmarks of neurodegeneration (Wu et al., 2015). In nature, *C. elegans* is found in environments particularly rich in microbes and have evolved mechanisms to differentiate between non-pathogenic and pathogenic bacteria. Sensory neurons and G-protein-coupled receptors (GPCRs) play a role in controlling innate immunity against bacterial infections (Cao et al., 2017; Singh and Aballay, 2009; Styer et al., 2008; Sun et al., 2011, 2017). Indeed, GPCRs present in the sensory neurons play an essential role in protecting the nematode from pathogenic bacteria by activating a flight-and-fight response that involves activation of microbicidal mechanisms and pathogen avoidance (Singh and Aballay, 2019).

Herein, we took a forward genetic approach to uncover regulatory mechanisms involved in the control of the effects of *P. aeruginosa* infection on the degeneration of chemosensory neurons in *C. elegans*. Chemosensory neurons are one of the first cell types that encounter external environment stimuli via surface receptors. We previously found that during pathogen infection the dendrites of the sensory neurons displayed degeneration phenotypes, including dendrite blebbing and dendrite branching (Wu et al., 2015). To identify genes involved in the control of these degeneration phenotypes, we conducted a screen to isolate mutants exhibiting enhanced susceptibility to

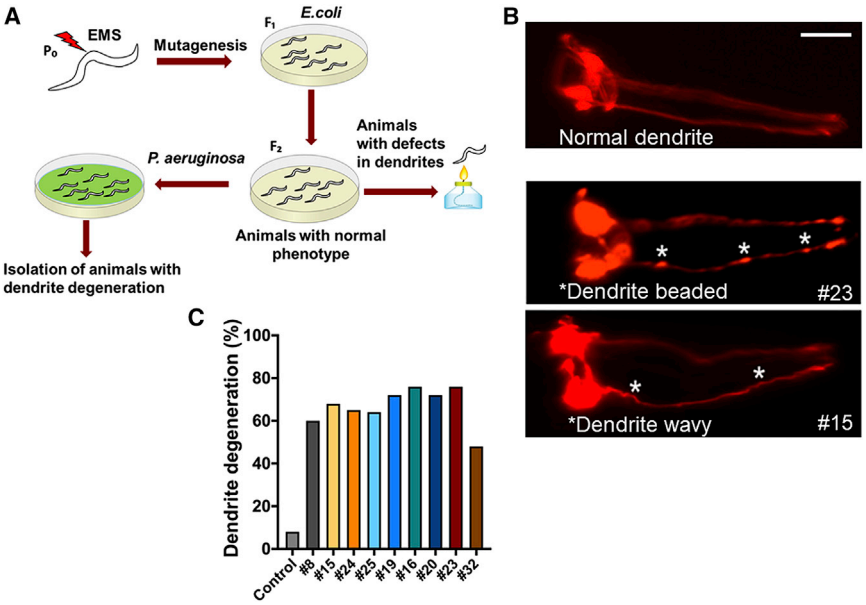

Figure 1. Forward Genetic Screen to Isolate Mutants Susceptible to Infection-Associated Dendrite Degeneration

(A) Schematic diagram of the forward genetic screen. Animals (P0) were treated with ethylmethanesulfonate (EMS) and the F1 animals were self-fertilized. The F2 animals were analyzed for dendrite degeneration, and animals exhibiting any changes were discarded. The remaining mutants were infected with *P. aeruginosa* for 24 h and screened for dendrite degeneration.

(B) Representative photomicrographs of dendrite degeneration in control animals expressing RFP under the control of *odr-1* promoter (CX5974) (top panel) and two representative mutants (#23 and #15) (bottom panels) after exposed to *P. aeruginosa* for 24 h. The scale bars represent 20 μm. White asterisk indicates bead-like structures and wavy dendrites.

(C) Quantification of dendrite degeneration in control and different mutant animals after 24 h of infection.

infection-associated dendrite degeneration. We identified a mutant carrying a mutation in the *srbc-48* gene, which was susceptible to infection-associated dendrite degeneration. The gene *srbc-48* belongs to a secretin-like (class B) family of GPCRs. GPCRs are the largest membrane-bound protein family and more than half of all drugs target these receptors (Lagerström and Schiöth, 2008). They have important roles in physiological processes, including pain sensation, tumorigenesis, inflammation, metabolic disorders, and neurotransmission. The secretin family of GPCRs, specifically, represents important drug targets for therapeutics against neurodegeneration, diabetes, and stress (Bortolato et al., 2014; Hollenstein et al., 2014).

We found that the *srbc-48* gene is expressed in olfactory AWC neurons where it plays a protective role by preventing pathogen-mediated deleterious effects on both neural integrity and the lifespan of the animals. The mutation in this receptor resulted in enhanced infection-associated dendrite degeneration and the hyperactivation of the DAF-16/FOXO transcription factor. Our data suggest that hyperactivation of DAF-16 in *srbc-48* animals, which resulted in the uncontrolled expression of immune genes, may ultimately decrease longevity. Thus, our findings uncover a role of SRBC-48 in protecting animals from infection-associated degeneration in a cell-autonomous manner. They also indicate that dendrite degeneration caused by an infection early in life may negatively impact the lifespan of animals.

RESULTS

SRBC-48 Protects against Infection-Associated Dendrite Degeneration

To identify the genes that play a role in the neurodegenerative changes induced by infection with *P. aeruginosa*, we conducted a forward genetic screen for mutants exhibiting an enhanced infection-associated dendrite degeneration (IADD) phenotype. The strain used, CX5974, takes advantage of the *odr-1* promoter to express red fluorescent protein (RFP) in AWC, AWB, and I1 neurons (Chen et al., 2011). Each of the two AWC neurons, AWCL, and AWCR, are sensory neurons with ciliated sheet-like endings and association with amphid sheath. We screened approximately 80,000 mutagenized haploid genomes resulting in the selection of 17 mutants exhibiting changes in the morphology of the dendrites after 24 h of *P. aeruginosa* infection (Figure 1A). These mutants showed significant changes in the morphology of the dendrites in terms of the bead and blebbing like structures compared to CX5974 control animals (Figure 1B). Some of the mutants also exhibited waviness in the dendrite structure. Mutants showing strong IADD phenotypes after being backcrossed six times (Figure 1C) were sequenced.

After subtraction of the common variants, linkage maps of single-nucleotide polymorphisms (SNPs) were obtained (Figure S1). Further analysis of the mapped region of mutant number 23 revealed a single C→T mutation in the GPCR *srbc-48* gene in the *C. elegans* genome that results in a serine-to-phenylalanine substitution at residue 280. As shown in Figure 2A, the AWC cells of *srbc-48(ac23)* animals exhibited blebbed and beaded dendrites, which are hallmarks of neurodegeneration, after only 24 h of exposure to *P. aeruginosa*, while those changes were not observed in control animals. Only animals exhibiting blebbing or bead-like structures along the length of the dendrite were scored as having infection-associated dendrite degeneration. While 76% of the *srbc-48(ac23)* animals exhibited the dendrite degeneration phenotype, only 8% of the control animals exhibited the phenotype (Figure 2B). To address whether the dendrite degeneration observed in the AWC cells of *srbc-48(ac23)* animals affected the function of the cells, we studied the chemotaxis of infected animals toward the chemoattractant benzaldehyde. As shown in Figure 2C, *srbc-48(ac23)* animals exhibited a significant reduction in chemotaxis compared to

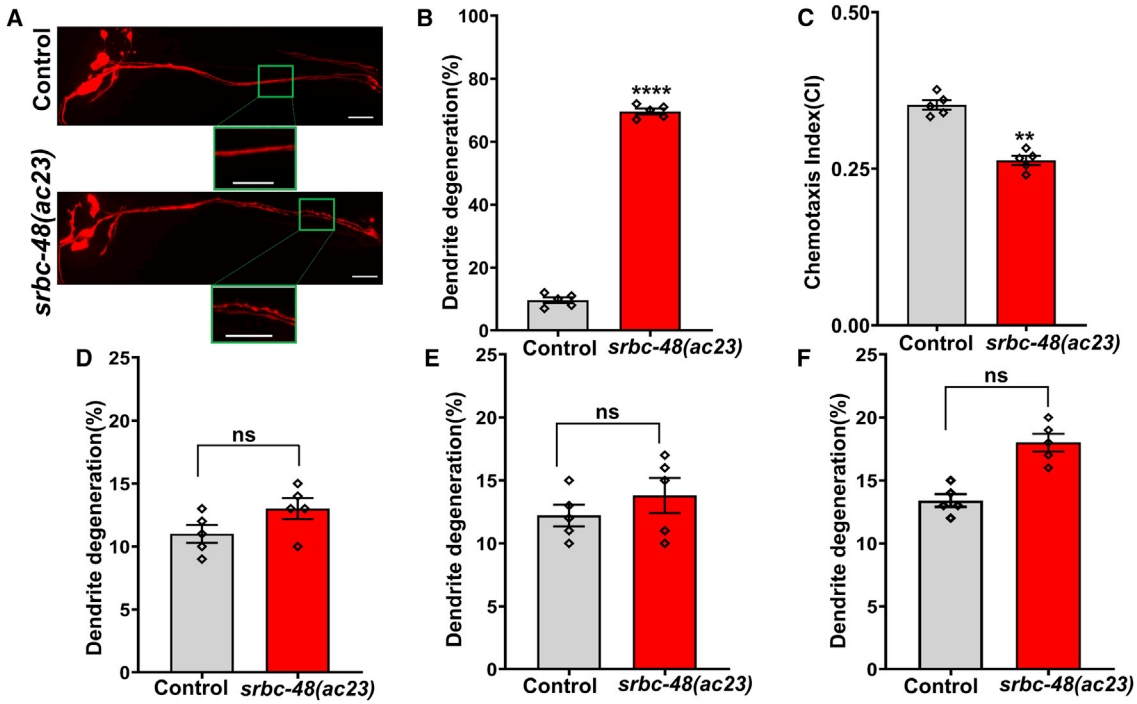

Figure 2. *srbc-48(ac23)* Animals Are Susceptible to Infection-Associated Dendrite Degeneration

(A) Representative photomicrographs of dendrite degeneration in control (CX5974) and *srbc-48(ac23)* animals after exposure to *P. aeruginosa* for 24 h. The scale bars represent 20 μm.

(B) Quantification of dendrite degeneration in control and *srbc-48(ac23)* animals. Control versus *srbc-48(ac23)* ($p < 0.0001$) via t test (n = 5; animals per condition = 50).

(C) Quantification of chemotaxis index (CI) in control and *srbc-48(ac23)* animals in response to benzaldehyde. Control versus *srbc-48(ac23)* ($p < 0.01$) via t test (n = 5; animals per condition > 100).

(D) Quantification of dendrite degeneration in control and *srbc-48(ac23)* animals after exposure to *E. faecalis* for 24 h. Control versus *srbc-48(ac23)* (n.s.) via t test (n = 5; animals per condition = 20).

(E) Quantification of dendrite degeneration in control and *srbc-48(ac23)* animals in response to cold stress. Control versus *srbc-48(ac23)* (n.s.) via t test (n = 5; animals per condition = 20).

(F) Quantification of dendrite degeneration in control and *srbc-48(ac23)* animals in response to osmotic stress. Control versus *srbc-48(ac23)* (n.s.) (n = 5; animals per condition = 20) via t test.

(B–F) The rhomboids represent individual experiments.

control animals, indicating that the function of AWC neurons is defective.

We also studied the morphological changes in AWC dendrites in *srbc-48(ac23)* animals exposed to the Gram-positive pathogen *Enterococcus faecalis* or insults like cold and osmotic stress. We found that exposure to *E. faecalis* for 24 h did not induce any dendrite degeneration in the *srbc-48(ac23)* mutants compared to control animals (Figure 2D). To study whether cold stress induces dendrite degeneration, control and *srbc-48(ac23)* animals were exposed to 4°C for 24 h. As shown in Figure 2E, although the number of *srbc-48(ac23)* animals exhibiting morphological changes in the dendrites was higher than that of control animals, the differences were not significant. We also studied the susceptibility of *srbc-48(ac23)* and control animals to another non-pathogen stressor, osmotic stress. Mutants and control animals were exposed to 500 mM sodium chloride (NaCl) to cause osmotic stress and then were observed for changes in the morphology of the dendrites. As in the case of cold stress, *srbc-48(ac23)* mutants exhibited a trend toward higher dendrite degeneration than control animals (Figure 2F). However, the trend was neither significant nor was it nearly as strong as the dendrite degeneration induced by *P. aeruginosa* infection (Figure 2B). Overall, these results indicate that *srbc-48(ac23)* animals are not necessarily susceptible to dendrite degeneration caused by stress in general.

Gene *srbc-48* Acts Cell Autonomously to Regulate Infection-Associated Dendrite Degeneration

To confirm that the absence of *srbc-48* caused the *srbc-48(ac23)* animals to become susceptible to infection-associated dendrite degeneration, we created *srbc-48(ac23)* animals expressing *srbc-48* under its own promoter (strain AY145). As shown in Figures 3A and 3B, the IADD phenotype of *srbc-48(ac23)* animals was completely rescued in these animals.

To determine the expression pattern of the *srbc-48* gene, we expressed GFP driven by the 4-kb promoter of the *srbc-48* gene in control animals that expressed RFP under the *odr-1* promoter. The transgene *srbc-48::gfp* was expressed in head

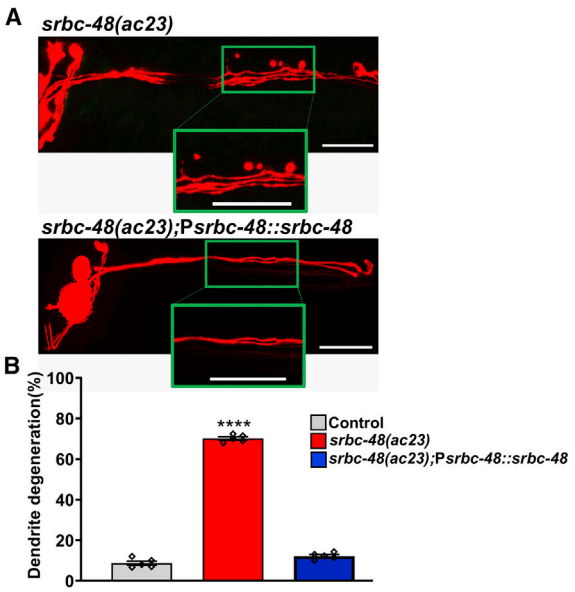

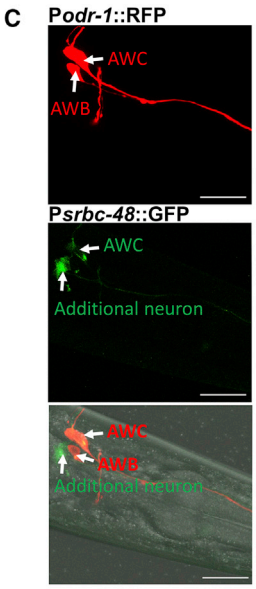

Figure 3. Expression of the Gene *srbc-48* Rescues the Infection-Associated Dendrite Degeneration Phenotype of *srbc-48(ac23)* Mutants

(A) Representative photomicrographs of dendrite degeneration after exposed to *P. aeruginosa* for 24 h in *srbc-48(ac23)* animals and animals expressing *srbc-48* under its own promoter, strain AY145 (*srbc-48(ac23);*P*srbc-48::srbc-48).* The scale bars represent 20 μm.

(B) Quantification of the dendrite degeneration phenotype in control, *srbc-48(ac23)*, and strain AY145 (*srbc-48(ac23);*P*srbc-48::srbc-48)* animals. The black symbols represent individual experiments (n = 5; animals per condition = 50). Control versus *srbc-48(ac23)* ($p < 0.0001$) and *srbc-48(ac23)* versus strain AY145 ($p < 0.0001$) via one-way ANOVA test.

(C) Representative photomicrographs of animals expressing RFP under the control of the *odr-1* promoter and GFP under the *srbc-48* promoter. The bottom panel corresponds to the merged images. The scale bars represent 20 μm.

neurons that were likely to be AWC neurons and one additional neuron (Figure 3C). Thus, we reasoned that SRBC-48 could have cell-autonomous or non-cell-autonomous effects in infection-associated dendrite degeneration. To distinguish between these possibilities, we used 4 kb of the *odr-1* promoter to express *srbc-48* in the AWC neurons but not in the additional neuron that also expresses *srbc-48*. As shown in Figures 4A and 4B, *srbc-48(ac23)* animals expressing *srbc-48* under the *odr-1* promoter (AY146) showed full rescue of the IADD phenotype.

Next, we tested whether *srbc-48* could function in a non-cell-autonomous manner to prevent infection-associated dendrite degeneration in different types of neurons. Thus, we analyzed dendrite degeneration in the PVD and AWB neurons of *srbc-48(ac23)* animals. PVD neurons are mechanosensory neurons that show age-related morphological changes in their dendrites (Kravtsov et al., 2017), and AWB are chemosensory neurons that are in close proximity to AWC neurons. We did not observe any signs of dendrite degeneration in the PVD and AWB neurons of *srbc-48(ac23)* animals after exposure to *P. aeruginosa* for 24 h (Figures 4C and 4D). Taken together, these results suggest *srbc-48* functions cell autonomously to protect AWC neurons from infection-associated dendrite degeneration.

Infection-Associated Dendrite Degeneration Decreases Animal Longevity in *srbc-48* Animals

Because it has been shown that inhibition of *str-2*, which is a GPCR expressed in the AWC neurons, extends lifespan (Alcedo and Kenyon, 2004), we decided to investigate whether *srbc-48(ac23)* animals exhibited any abnormal longevity. We did not find any differences in the lifespan of control and *srbc-48(ac23)* animals in the absence of infection or after 8 h of infection (Figures 5A and 5B). These results were expected as the AWC dendrites of *srbc-48(ac23)* animals do not exhibit degeneration in the absence of an infection. However, we reasoned that a short infection by *P. aeruginosa* that is insufficient to cause death but sufficient to cause dendrite degeneration might alter the longevity of *srbc-48(ac23)* animals. To test this hypothesis, we performed an acute *P. aeruginosa* infection by only exposing the animals to the pathogen for 12 and 24 h. To remove any live *P. aeruginosa*, the animals were rinsed with a buffer containing antibiotics before transferring them to plates that contained antibiotics and were seeded with killed *E. coli* (Head et al., 2017). As shown in Figures 5C and 5D, there was a significant decrease in the lifespan of *srbc-48(ac23)* animals infected for 12 and 24 h with *P. aeruginosa* compared to control animals.

We observed a decrease in the lifespan of *srbc-48(ac23)* animals infected for only 12 h with *P. aeruginosa* (Figure 5C), but we only observed significant dendrite degeneration 24 h after infection (Figures 2A and 2B). Therefore, we asked whether only 12 h of *P. aeruginosa* infection was sufficient to induce dendrite degeneration later in life, even in the absence of the pathogen. Animals exposed to *P. aeruginosa* for only 12 h developed dendrite degeneration 12 h later (Figures S2A and S2B), which is consistent with the reduced longevity of animals infected for only 12 h (Figure 5C) and suggests that infection-associated dendrite degeneration is irreversible. To test this hypothesis, we analyzed dendrite degeneration in *srbc-48(ac23)* animals at 1, 3, and 5 days after the infection with *P. aeruginosa* has been cleared and found that dendrite degeneration continued to increase (Figure S2C). These results indicate that the infection-associated dendrite degeneration caused by infection with *P. aeruginosa* for only 12 or 24 h results in a reduction of the longevity of *srbc-48(ac23)* animals.

Because expression of *srbc-48* under the control of its own promoter or the *odr-1* promoter rescued the dendrite degeneration phenotype induced by *P. aeruginosa* infection, we next sought to address whether *srbc-48* expression could rescue the decrease in longevity caused by *P. aeruginosa* infection early

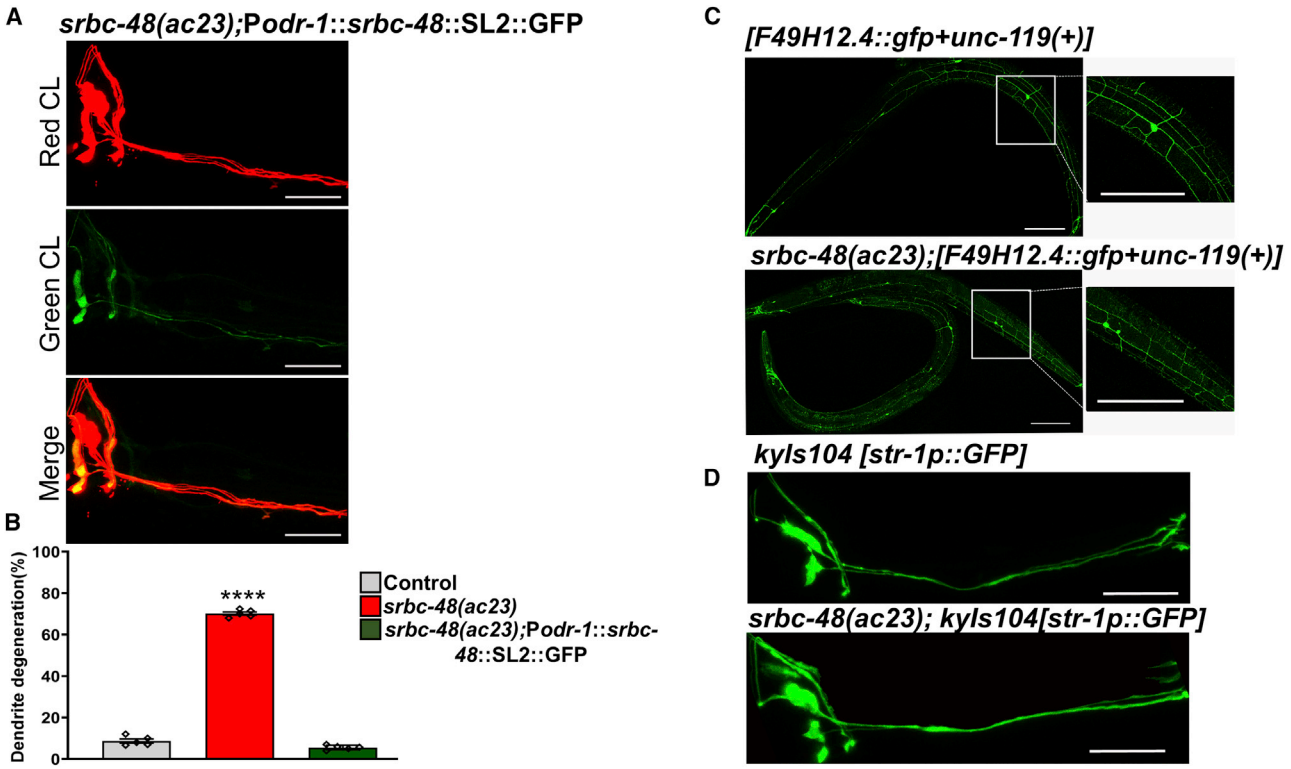

Figure 4. *srbc-48* Mutation Enhances that Animal Susceptibility to Infection-Associated Dendrite Degeneration in a Cell-Autonomous Manner

(A) Representative photomicrographs of *srbc-48* animals expressing *srbc-48* and *gfp* under the control of the *odr-1* promoter, strain AY146 (*srbc-48(ac23);*P*odr-1*::*srbc-48*::SL2::GFP), after 24 h of *P. aeruginosa* infection. The scale bars represent 20 μm.

(B) Quantification of the dendrite degeneration phenotype in control, *srbc-48(ac23)*, and strain AY146 (*srbc-48(ac23);*P*odr-1*::*srbc-48*::SL2::GFP) animals. The black symbols represent individual experiments (n = 5; animals per condition = 50). Control versus *srbc-48(ac23)* ($p < 0.0001$) and *srbc-48(ac23)* versus strain AY146 ($p < 0.0001$) via one-way ANOVA test.

(C) Representative photomicrographs of strain NC1686 (wdIs51), which expresses GFP in PVD neurons, crossed with *srbc-48(ac23)* animals after exposure to *P. aeruginosa* for 24 h (n = 3; animals per condition = 20). The scale bars represent 100 μm.

(D) Representative photomicrographs of strain CX3553 (*kyIs104*), which expresses GFP in AWB neurons, crossed with *srbc-48(ac23)* animals after exposure to *P. aeruginosa* for 24 h (n = 3; animals per condition = 20). The scale bars represent 20 μm.

in the life of *srbc-48(ac23)* animals. As shown in Figure 5D, expression of *srbc-48* fully rescued the decreased longevity of *srbc-48(ac23)* animals caused by an infection early in life, indicating that defective AWC cells reduce lifespan. Consistent with this idea, we found that pathogen infection reduced the lifespan of both AWC ablated and *srbc-48(ac23)* animals to a similar extent (Figure S3A).

We then studied the susceptibility to *P. aeruginosa* of the animals. We observed that there was no significant change in the survival of the control and the *srbc-48(ac23)* animals constantly exposed to *P. aeruginosa* (Figure S4A). Similar results were obtained with animals infected with *E. faecalis* (Figure S4B). Taken together, these results indicate that *srbc-48(ac23)* animals are not susceptible to pathogen infection, suggesting that the deleterious effects of *P. aeruginosa* infection on dendrites is not a consequence of the premature death of the infected animals or due to the animals being sickly. The results also suggest that SRBC-48 and AWC control pathways play an important role in the control of longevity.

Infection-Associated Dendrite Degeneration Increases Gene Expression of Immune Genes

To elucidate the mechanism by which infection-associated dendrite degeneration decreases longevity in *srbc-48(ac23)* animals compared to control animals, we studied changes in gene expression after 24 h of infection with *P. aeruginosa*. We crossed both control and *srbc-48(ac23)* animals with sterile *fer-1* animals to avoid the collection of RNA from the progeny. Only differentially expressed genes with p-adj < 0.05 were considered to avoid false discovery rate, and for the upregulated genes, only those having a fold change >2-fold were taken into account (Tables S1, S2, and S3). An unbiased gene enrichment analysis using the Database for Annotation, Visualization, and Integrated Discovery (DAVID) (https://david.ncifcrf.gov/) (Huang et al., 2009) showed that the innate immune Gene Ontology (GO) cluster is among the groups with the most hits. Other GO clusters correspond to ion, acetylcholine, glutamate, and chloride transport genes, neuropeptide signaling pathway, and signal transduction (Figure 6A; Table S4).

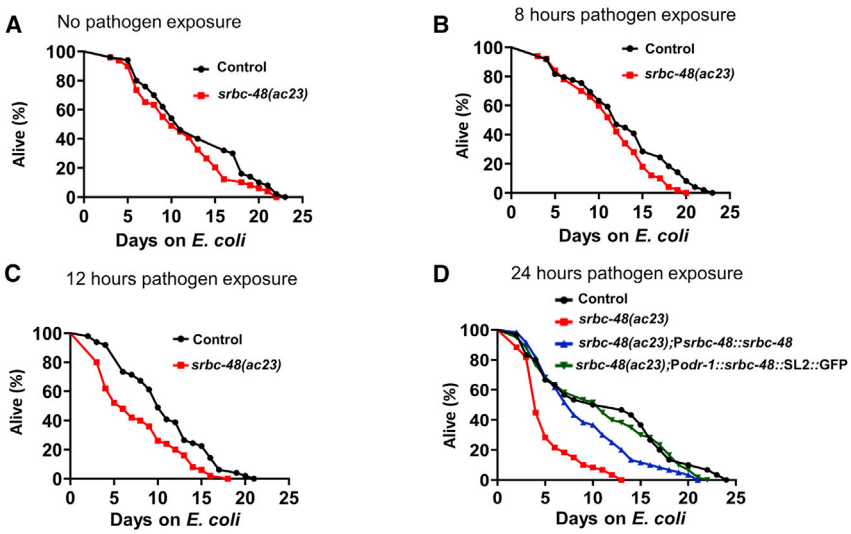

Figure 5. Pathogen Infection in *srbc-48* Animals Results in a Reduced Lifespan

(A) Representative lifespan plots of control and *srbc-48*(*ac23*) without infection. Control versus *srbc-48*(*ac23*) (n.s.).

(B) Representative lifespan plots of control and *srbc-48*(*ac23*) animals after 8 h of *P. aeruginosa* exposure. Control versus *srbc-48*(*ac23*) (n.s.).

(C) Representative lifespan plots of control and *srbc-48*(*ac23*) after 12-h *P. aeruginosa* exposure. Control versus *srbc-48*(*ac23*) ($p < 0.001$).

(D) Representative lifespan plots of control, *srbc-48*(*ac23*), and rescued strains AY145(*srbc-48(ac23);*P*srbc-48::srbc-48)* and AY146 (*srbc-48(ac23);*P*odr-1*::*srbc-48*::SL2::GFP) after 24 h of *P. aeruginosa* exposure. Control versus *srbc-48*(*ac23*) ($p < 0.0001$), *srbc-48(ac23)* versus strain AY145 ($p < 0.0001$), *srbc-48*(*ac23*) versus strain AY146 ($p < 0.0001$), control versus strain AY145 (n.s.), and control versus strain AY146 (n.s.) ($n = 3$; animals per condition = 100).

To analyze more in depth the innate immunity cluster, we compared this cluster of genes to previously identified gene sets that are known to be controlled by various signaling pathways and transcription factors involved in *C. elegans* response against pathogen infection (Table S5). We found a significant overlap between genes upregulated in *srbc-48(ac23)* animals infected with *P. aeruginosa* and gene sets regulated by DAF-16/FOXO, CEP-1, and SKN-1 (Figure 6B). We further confirmed the RNA-sequencing results by selecting the genes from pathways with maximum overlap and performing quantitative real-time PCR (Figure 6C). Our analysis suggests that the decreased longevity that *srbc-48* animals exhibit after exposure to *P. aeruginosa* may be a consequence of uncontrolled activation of immune pathways.

Infection-Associated Dendrite Degeneration Possibly Decreases Lifespan of *srbc-48* Animals by Hyperactivating DAF-16

The insulin/insulin-like growth factor (IGF)-1 receptor homolog DAF-2 and its main target, DAF-16, play an important role in the regulation of lifespan at least in part by controlling immune gene expression (Garsin et al., 2003; Lee et al., 2003; Murphy et al., 2003). Because our gene expression studies indicate that there is a significant enrichment of DAF-16 controlled genes in infected *srbc-48(ac23)* animals and excessive DAF-16 activity may have deleterious consequences (Singh and Aballay, 2009), we investigated DAF-16 activation. Like mammalian FOXO3a, the activity of DAF-16 is tightly regulated by a wide variety of external stimuli, including different stresses, that result in its nuclear localization (Brunet et al., 2004; Henderson and Johnson, 2001; Lin et al., 2001). As shown in Figures 7A and 7B, *srbc-48(ac23)* animals showed an extensive DAF-16 nuclear localization after 24 h of *P. aeruginosa* infection that was absent in control animals. To address whether the increased DAF-16 nuclear localization exhibited by *srbc-48(ac23)* animals is reversible, we studied DAF-16 localization 10 days after the animals were cleared from *P. aeruginosa* and transferred to *E. coli*. As shown in Figures S5A and S5B, DAF-16 remains in the nuclei of *srbc-48(ac23)* animals, which suggests that DAF-16 inactivation is deficient in these animals. Given that the decrease in longevity of *srbc-48(ac23)* animals was rescued by the expression of *srbc-48* under the control of the *odr-1* promoter that drives its expression to AWC (Figure 5D), we reasoned that we should also observe rescue of DAF-16 nuclear localization in *srbc-48(ac23)* animals expressing *srbc-48* in AWC. We found that DAF-16 relocalized to the cytosol 5 days after infection with *P. aeruginosa* in the rescued animals (Figures S5C and S5D). These findings indicate that a defect in AWC neuron structure and function causes an irreversible DAF-16/FOXO nuclear localization induced by *P. aeruginosa* that results in a reduced lifespan long after the infection has been cleared.

We hypothesized that if the infection-associated dendrite degeneration in *srbc-48* animals that results in the activation of DAF-16 is responsible for their reduced longevity, DAF-16 inhibition should improve their longevity. Consistent with this idea, we found that RNAi inactivation of *daf-16* suppressed the reduced lifespan of *srbc-48(ac23)* animals that were infected with *P. aeruginosa* as young adults (Figure 7C). In contrast, RNAi inactivation of *cep-1* decreased the lifespan of both *srbc-48(ac23)* and control animals (Figure 7D). The rescue in lifespan after *daf-16* knockdown was further confirmed by using *daf-16(mu86)* mutant animals (Figure 7E). The rescue in lifespan by *daf-16* inactivation suggests that the dendrite degeneration suffered by *srbc-48(ac23)* animals due to infection early in their life may result in a decreased longevity due to hyperactivation of DAF-16.

DISCUSSION

Although there are differences between the *C. elegans* and mammalian nervous system, several studies have shown that genes linked to neurodegenerative diseases in humans have

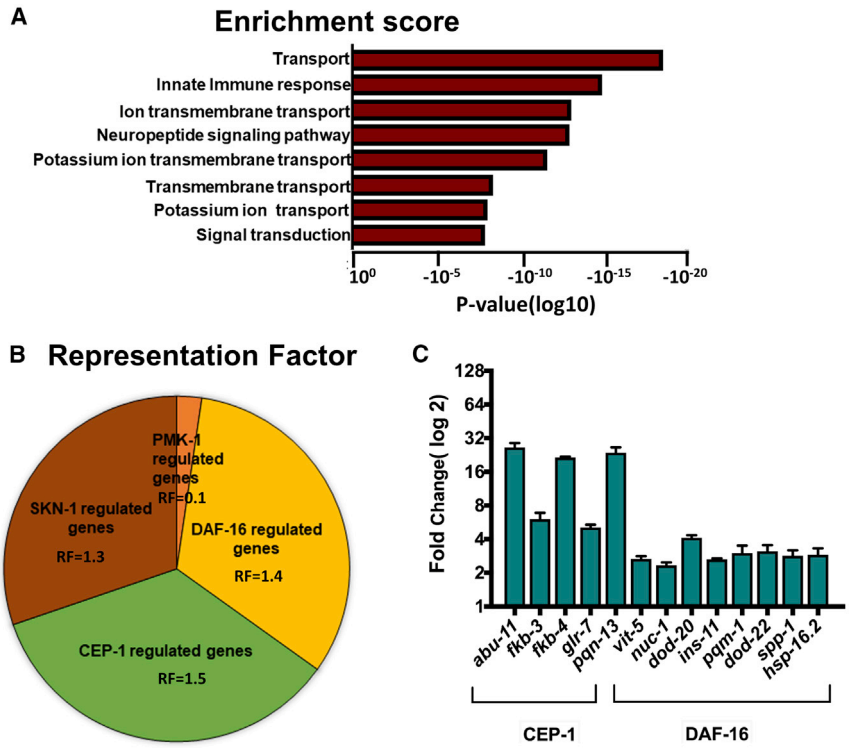

Figure 6. RNA-Sequencing Analysis of the Upregulated Genes Showed an Enrichment for Immune Genes as well as Overlap with the Genes Regulated by DAF-16

(A) Enrichment score of the upregulated genes in *srbc-48(ac23)* animals compared to control animals.

(B) Graphical representation of the representation factor of the upregulated genes that are controlled by the PMK-1, DAF −16, CEP-1, and SKN-1 pathways.

(C) Quantitative real-time PCR analysis of CEP-1 and DAF-16-dependent genes in *srbc-48(ac23)* compared with control animals (n = 3; three technical replicates in each case).

C. elegans homologs. These genes when mutated or deleted result in strong degeneration phenotypes in *C. elegans* neurons, demonstrating the remarkable similarity between the two systems in terms of connectivity and functionality (Alexander et al., 2014; Faber et al., 2002; Fang et al., 2019; Harrington et al., 2010). Here, we show that *P. aeruginosa* infection induces dendrite degeneration in the AWC neurons of *C. elegans*. Dendrites have an essential role in the function of neuronal circuits, and dendrite degeneration is reported in neurodegenerative and cognitive disorders (Kweon et al., 2017; Kwon et al., 2018). Studies have also shown that microbial pathogens can trigger neurodegenerative diseases and associated symptoms, including inflammation and memory deficits in Alzheimer patients (Itzhaki et al., 2016).

The underlying mechanisms responsible for infection-associated dendrite degeneration are unclear. To gain insight into the mechanisms responsible for this phenomenon, we performed a forward genetics screen to discover genes involved in infection-associated dendrite degeneration. We studied dendrite degeneration in the sensory neurons because chemoperception is used in *C. elegans* to distinguish pathogenic from non-pathogenic bacteria. Sensory neurons are the first neural cells to encounter external cues and they play an essential role in regulating immune responses during pathogen exposure. Our forward genetic screen identified animals that carry a mutation in the gene *srbc-48*, which makes them susceptible to dendrite degeneration induced by *P. aeruginosa* infection at earlier time points after infection. The lack of pathogen susceptibility of *srbc-48(ac23)* animals indicates that the observed dendrite degeneration is not a consequence of the animals being sickly or their premature death. While we did not observe dendrite degeneration in *srbc-48(ac23)* animals infected with *E. faecalis* for 24 h, other pathogens should be studied to address the pathogen specificity of the susceptibility of *srbc-48(ac23)* animals to infection-associated dendrite degeneration. However, the infection-associated dendrite degeneration due to *srbc-48* mutation seems to be specific to AWC neurons as no dendrite degeneration was observed in AWB neurons, which are also chemosensory. Neither did we observe dendrite degeneration in PVD neurons, which undergo age-related degeneration. This suggests that *srbc-48* is involved in infection-associated dendrite degeneration in AWC neurons, and that this occurs independently of aging. Additionally, dendrite degeneration of AWC neurons in the absence of functional SRBC-48 suggests that this GPCR has a neuroprotective role during *P. aeruginosa* infection.

We also found that infection-associated dendrite degeneration negatively impacted the lifespan of the animals. Sensory perception plays an important role in the control of lifespan in *C. elegans* (Alcedo and Kenyon, 2004; Apfeld and Kenyon, 1999), as GPCRs present in the sensory neurons detect olfaction and taste cues to activate other G protein-mediated signaling cascades (Troemel et al., 1995). To decipher the relationship between dendrite degeneration and decreased lifespan, we studied changes in gene expression in animals susceptible to infection-associated dendrite degeneration. We found that the immune response genes were among the most enriched cluster of genes upregulated in *srbc-48(ac23)* animals and that many of them are controlled by DAF-16, which plays an essential role in lifespan regulation. We also found that there was enhanced nuclear translocation of DAF-16 in *srbc-48(ac23)* animals after *P. aeruginosa* infection and that these animals were deficient in DAF-16 inactivation. Inhibition of *daf-16* through RNAi or mutation suppressed the reduced lifespan of *srbc-48(ac23)* animals that suffered pathogen-mediated dendrite degeneration, suggesting that DAF-16 hyperactivity may be responsible for their decreased lifespan. Even though *srbc-48(ac23)* animals exhibit higher expression of immune genes, they are not more resistant

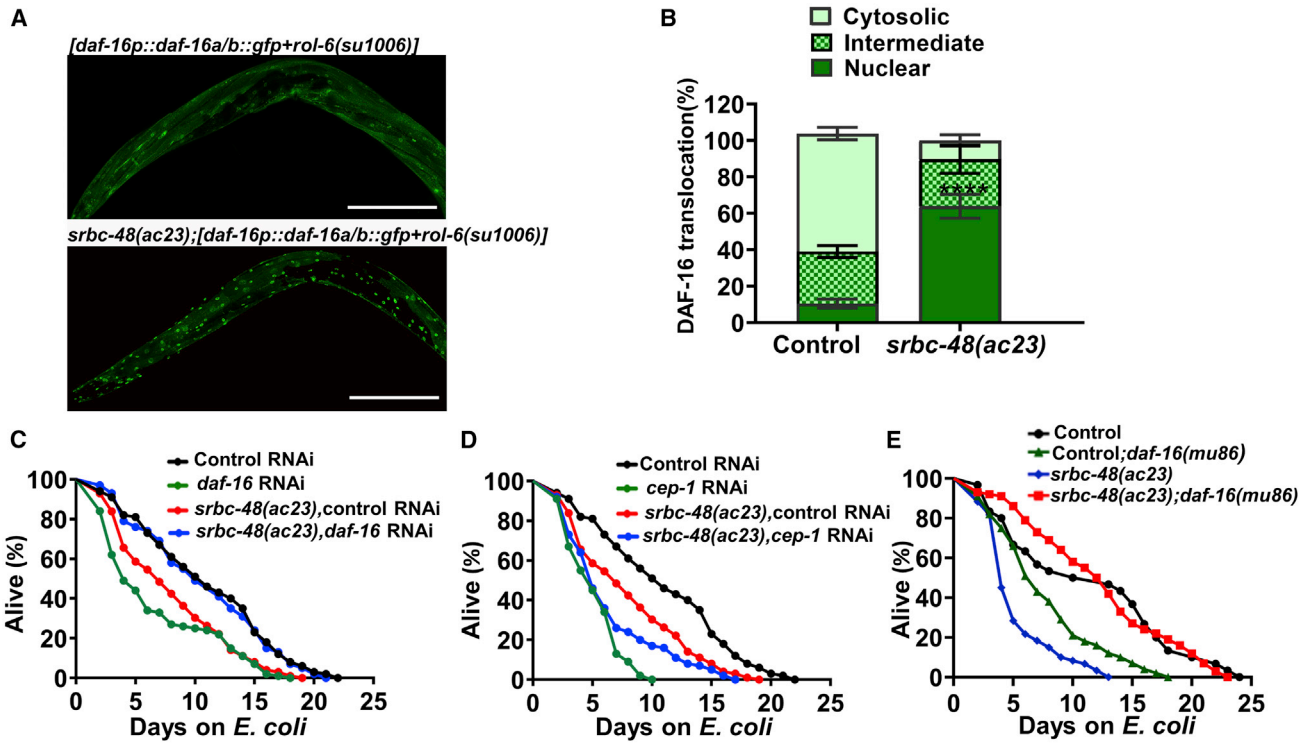

Figure 7. Inactivation of DAF-16 Rescues the Decreased Lifespan of *srbc-48(ac23)* Animals that Suffered an Infection Early in Life

(A) Representative mosaic photomicrographs of DAF-16::GFP nuclear localization in control *[daf-16p::daf-16a/b::gfp+rol-6(su1006)]* and mutant *srbc-48(ac23);[daf-16p::daf-16a/b::gfp+rol-6(su1006)]* animals after exposed to *P. aeruginosa* for 24 h. The scale bars represent 100 μm.

(B) Quantification of DAF-16 nuclear localization in control *[daf-16p::daf-16a/b::gfp+rol-6(su1006)]* and mutant *srbc-48(ac23);[daf-16p::daf-16a/b::gfp+rol-6(su1006)]* animals (n = 3; animals per condition = 20). Nuclear translocation of control versus *srbc-48(ac23)* ($p < 0.0001$), one-way ANOVA test.

(C) Representative lifespan plots of control and *srbc-48(ac23)* animals after knockdown of *daf-16* via RNAi followed by 24-h exposure to *P. aeruginosa* (n = 3; animals per condition = 100). *srbc-48(ac23)* control RNAi versus *srbc-48(ac23);daf-16* RNA ($p < 0.0001$).

(D) Representative lifespan plots of control and *srbc-48(ac23)* animals after knockdown of *cep*-1 via RNAi followed by 24-h exposure to *P. aeruginosa* (n = 3; animals per condition = 100). *srbc-48(ac23)* control RNAi versus *srbc-48(ac23);cep-1* RNAi ($p < 0.01$).

(E) Representative lifespan plots of control, *srbc-48(ac23)*, control;*daf-16(mu86)*, and *srbc-48(ac23);daf-16(mu86)* animals after 24-h *P. aeruginosa* exposure (independent replicates, n = 3; animals per condition, n = 100). *srbc-48(ac23)* versus *srbc-48(ac23);daf-16(mu86)* ($p < 0.0001$), control versus control;*daf-16(mu86)* ($p < 0.0001$), control;*daf-16(mu86)* versus *srbc-48(ac23);daf-16(mu86)* ($p < 0.0001$), and control versus *srbc-48(ac23);daf-16(mu86)* (n.s.).

to pathogen-mediated killing. Our lifespan studies suggest that DAF-16 hyperactivity is deleterious. Thus, it is possible that the overall activation of immune genes exhibited by *srbc-48(ac23)* animals is dampened by the harmful effects of excessive DAF-16 activity.

In conclusion, our study suggests a cell-autonomous role of the neuronal GPCR, *srbc-48*, in protecting against infection-associated dendrite degeneration. Our study provides insights into the integration between the chemosensory system and the insulin-signaling pathway. The protective function of SRBC-48 against dendrite degeneration caused by pathogen infection was found to be critical to prevent the DAF-16 hyperactivation, establishing a link between infection-associated dendrite degeneration and longevity.

STAR★METHODS

Detailed methods are provided in the online version of this paper and include the following:

- RNA Interference (RNAi)
- Assay for DAF-16 Nuclear Localization
- Chemotaxis Assay
- RNA Isolation and Quantitative Real-Time PCR
- RNA Sequencing and Gene Expression Analysis

- QUANTIFICATION AND STATISTICAL ANALYSIS

SUPPLEMENTAL INFORMATION

Supplemental Information can be found online at https://doi.org/10.1016/j.celrep.2020.107662.

ACKNOWLEDGMENTS

This work was supported by NIH grants AI117911 and GM070977 (to A.A.). *C. elegans* strains used in the study were provided by the *Caenorhabditis* Genetics Center (CGC), which is funded by the NIH Office of Research Infrastructure Programs (P40 OD010440).

AUTHOR CONTRIBUTIONS

S.K. and A.A. conceived and designed the experiments. S.K. performed the experiments. S.K. and A.A. analyzed the data and wrote the paper.

DECLARATION OF INTERESTS

The authors declare no competing interests.

Received: October 21, 2019
Revised: March 6, 2020
Accepted: April 28, 2020
Published: May 19, 2020

REFERENCES

Alcedo, J., and Kenyon, C. (2004). Regulation of C. elegans longevity by specific gustatory and olfactory neurons. Neuron *41*, 45–55.

Alexander, A.G., Marfil, V., and Li, C. (2014). Use of *C. elegans* as a model to study Alzheimer's disease and other neurodegenerative diseases. Front. Genet. *5*, 279.

Apfeld, J., and Kenyon, C. (1999). Regulation of lifespan by sensory perception in *Caenorhabditis elegans*. Nature *402*, 804–809.

Bortolato, A., Doré, A.S., Hollenstein, K., Tehan, B.G., Mason, J.S., and Marshall, F.H. (2014). Structure of class B GPCRs: new horizons for drug discovery. Br. J. Pharmacol. *171*, 3132–3145.

Brunet, A., Sweeney, L.B., Sturgill, J.F., Chua, K.F., Greer, P.L., Lin, Y., Tran, H., Ross, S.E., Mostoslavsky, R., Cohen, H.Y., et al. (2004). Stress-dependent regulation of FOXO transcription factors by the SIRT1 deacetylase. Science *303*, 2011–2015.

Caldwell, K.A., Tucci, M.L., Armagost, J., Hodges, T.W., Chen, J., Memon, S.B., Blalock, J.E., DeLeon, S.M., Findlay, R.H., Ruan, Q., et al. (2009). Investigating bacterial sources of toxicity as an environmental contributor to dopaminergic neurodegeneration. PLoS ONE *4*, e7227.

Camara-Lemarroy, C.R., Metz, L.M., and Yong, V.W. (2018). Focus on the gut-brain axis: multiple sclerosis, the intestinal barrier and the microbiome. World J. Gastroenterol. *24*, 4217–4223.

Cao, W., and Zheng, H. (2018). Correction to: peripheral immune system in aging and Alzheimer's disease. Mol. Neurodegener. *13*, 58.

Cao, X., Kajino-Sakamoto, R., Doss, A., and Aballay, A. (2017). Distinct roles of sensory neurons in mediating pathogen avoidance and neuropeptide-dependent immune regulation. Cell Rep. *21*, 1442–1451.

Chen, L., Fu, Y., Ren, M., Xiao, B., and Rubin, C.S. (2011). A RasGRP, *C. elegans* RGEF-1b, couples external stimuli to behavior by activating LET-60 (Ras) in sensory neurons. Neuron *70*, 51–65.

Cho, I., and Blaser, M.J. (2012). The human microbiome: at the interface of health and disease. Nat. Rev. Genet. *13*, 260–270.

Cook, S.J., Jarrell, T.A., Brittin, C.A., Wang, Y., Bloniarz, A.E., Yakovlev, M.A., Nguyen, K.C.Q., Tang, L.T.-H., Bayer, E.A., Duerr, J.S., et al. (2019). Whole-animal connectomes of both *Caenorhabditis elegans* sexes. Nature *571*, 63–71.

Derry, W.B., Bierings, R., van Iersel, M., Satkunendran, T., Reinke, V., and Rothman, J.H. (2007). Regulation of developmental rate and germ cell proliferation in Caenorhabditis elegans by the p53 gene network. Cell Death Differ. *14*, 662–670.

Faber, P.W., Voisine, C., King, D.C., Bates, E.A., and Hart, A.C. (2002). Glutamine/proline-rich PQE-1 proteins protect *Caenorhabditis elegans* neurons from huntingtin polyglutamine neurotoxicity. Proc. Natl. Acad. Sci. USA *99*, 17131–17136.

Fang, E.F., Hou, Y., Palikaras, K., Adriaanse, B.A., Kerr, J.S., Yang, B., Lautrup, S., Hasan-Olive, M.M., Caponio, D., Dan, X., et al. (2019). Mitophagy inhibits amyloid-β and tau pathology and reverses cognitive deficits in models of Alzheimer's disease. Nat. Neurosci. *22*, 401–412.

Garsin, D.A., Villanueva, J.M., Begun, J., Kim, D.H., Sifri, C.D., Calderwood, S.B., Ruvkun, G., and Ausubel, F.M. (2003). Long-lived *C. elegans* daf-2 mutants are resistant to bacterial pathogens. Science *300*, 1921.

Harrington, A.J., Hamamichi, S., Caldwell, G.A., and Caldwell, K.A. (2010). *C. elegans* as a model organism to investigate molecular pathways involved with Parkinson's disease. Dev. Dyn. *239*, 1282–1295.

Head, B.P., Olaitan, A.O., and Aballay, A. (2017). Role of GATA transcription factor ELT-2 and p38 MAPK PMK-1 in recovery from acute *P. aeruginosa* infection in *C. elegans*. Virulence *8*, 261–274.

Heintz, C., and Mair, W. (2014). You are what you host: microbiome modulation of the aging process. Cell *156*, 408–411.

Henderson, S.T., and Johnson, T.E. (2001). daf-16 integrates developmental and environmental inputs to mediate aging in the nematode *Caenorhabditis elegans*. Curr. Biol. *11*, 1975–1980.

Heneka, M.T., Kummer, M.P., and Latz, E. (2014). Innate immune activation in neurodegenerative disease. Nat. Rev. Immunol. *14*, 463–477.

Hill, J.M., Clement, C., Pogue, A.I., Bhattacharjee, S., Zhao, Y., and Lukiw, W.J. (2014). Pathogenic microbes, the microbiome, and Alzheimer's disease (AD). Front Aging Neurosci. *16*, 127.

Hollenstein, K., de Graaf, C., Bortolato, A., Wang, M.W., Marshall, F.H., and Stevens, R.C. (2014). Insights into the structure of class B GPCRs. Trends Pharmacol. Sci. *35*, 12–22.

Huang, W., Sherman, B.T., and Lempicki, R.A. (2009). Systematic and integrative analysis of large gene lists using DAVID bioinformatics resources. Nat. Protoc. *4*, 44–57.

Huang, W.S., Yang, T.Y., Shen, W.C., Lin, C.L., Lin, M.C., and Kao, C.H. (2014). Association between *Helicobacter pylori* infection and dementia. J. Clin. Neurosci. *21*, 1355–1358.

Itzhaki, R.F., Lathe, R., Balin, B.J., Ball, M.J., Bearer, E.L., Braak, H., Bullido, M.J., Carter, C., Clerici, M., Cosby, S.L., et al. (2016). Microbes and Alzheimer's disease. J. Alzheimers Dis. *51*, 979–984.

Kim, B.-S., Jeon, Y.-S., and Chun, J. (2013). Current status and future promise of the human microbiome. Pediatr. Gastroenterol. Hepatol. Nutr. *16*, 71–79.

Kravtsov, V., Oren-Suissa, M., and Podbilewicz, B. (2017). The fusogen AFF-1 can rejuvenate the regenerative potential of adult dendritic trees by self-fusion. Development *144*, 2364–2374.

Kweon, J.H., Kim, S., and Lee, S.B. (2017). The cellular basis of dendrite pathology in neurodegenerative diseases. BMB Rep. *50*, 5–11.

Kwon, M.J., Han, M.H., Bagley, J.A., Hyeon, D.Y., Ko, B.S., Lee, Y.M., Cha, I.J., Kim, S.Y., Kim, D.Y., Kim, H.M., et al. (2018). Coiled-coil structure-dependent interactions between polyQ proteins and Foxo lead to dendrite pathology and behavioral defects. Proc. Natl. Acad. Sci. USA *115*, E10748–E10757.

Lagerström, M.C., and Schiöth, H.B. (2008). Structural diversity of G protein-coupled receptors and significance for drug discovery. Nat. Rev. Drug Discov. *7*, 339–357.

Lee, S.S., Kennedy, S., Tolonen, A.C., and Ruvkun, G. (2003). DAF-16 target genes that control *C. elegans* life-span and metabolism. Science *300*, 644–647.

Leinwand, S.G., Yang, C.J., Bazopoulou, D., Chronis, N., Srinivasan, J., and Chalasani, S.H. (2015). Circuit mechanisms encoding odors and driving aging-associated behavioral declines in *Caenorhabditis elegans*. eLife *4*, e10181.

Lin, K., Hsin, H., Libina, N., and Kenyon, C. (2001). Regulation of the *Caenorhabditis elegans* longevity protein DAF-16 by insulin/IGF-1 and germline signaling. Nat. Genet. *28*, 139–145.

Mancuso, R., Baglio, F., Cabinio, M., Calabrese, E., Hernis, A., Nemni, R., and Clerici, M. (2014). Titers of herpes simplex virus type 1 antibodies positively correlate with grey matter volumes in Alzheimer's disease. J. Alzheimers Dis. *38*, 741–745.

Miklossy, J. (2011). Emerging roles of pathogens in Alzheimer disease. Expert Rev. Mol. Med. *13*, e30.

Minevich, G., Park, D.S., Blankenberg, D., Poole, R.J., and Hobert, O. (2012). CloudMap: a cloud-based pipeline for analysis of mutant genome sequences. Genetics *192*, 1249–1269.

Murphy, C.T., McCarroll, S.A., Bargmann, C.I., Fraser, A., Kamath, R.S., Ahringer, J., Li, H., and Kenyon, C. (2003). Genes that act downstream of DAF-16 to influence the lifespan of *Caenorhabditis elegans*. Nature *424*, 277–283.

Oh, S.W., Mukhopadhyay, A., Svrzikapa, N., Jiang, F., Davis, R.J., and Tissenbaum, H.A. (2005). JNK regulates lifespan in *Caenorhabditis elegans* by modulating nuclear translocation of forkhead transcription factor/DAF-16. Proc. Natl. Acad. Sci. USA *102*, 4494–4499.

Ohta, A., Ujisawa, T., Sonoda, S., and Kuhara, A. (2014). Light and pheromone-sensing neurons regulates cold habituation through insulin signalling in *Caenorhabditis elegans*. Nat. Commun. *5*, 4412.

Oliveira, R.P., Porter Abate, J., Dilks, K., Landis, J., Ashraf, J., Murphy, C.T., and Blackwell, T.K. (2009). Condition-adapted stress and longevity gene regulation by *Caenorhabditis elegans* SKN-1/Nrf. Aging Cell *8*, 524–541.

Oren-Suissa, M., Hall, D.H., Treinin, M., Shemer, G., and Podbilewicz, B. (2010). The fusogen EFF-1 controls sculpting of mechanosensory dendrites. Science *328*, 1285–1288.

Poole, S., Singhrao, S.K., Kesavalu, L., Curtis, M.A., and Crean, S. (2017). Determining the presence of periodontopathic virulence factors in short-term postmortem Alzheimer's disease brain tissue. J. Alzheimers Dis. *36*, 665–677.

Singh, V., and Aballay, A. (2009). Regulation of DAF-16-mediated innate immunity in *Caenorhabditis elegans*. J. Biol. Chem. *284*, 35580–35587.

Singh, J., and Aballay, A. (2019). Microbial colonization activates an immune fight-and-flight response via neuroendocrine signaling. Dev. Cell *49*, 89–99.e4.

Solomon, A., Bandhakavi, S., Jabbar, S., Shah, R., Beitel, G.J., and Morimoto, R.I. (2004). *Caenorhabditis elegans* OSR-1 regulates behavioral and physiological responses to hyperosmotic environments. Genetics *167*, 161–170.

Styer, K.L., Singh, V., Macosko, E., Steele, S.E., Bargmann, C.I., and Aballay, A. (2008). Innate immunity in *Caenorhabditis elegans* is regulated by neurons expressing NPR-1/GPCR. Science *322*, 460–464.

Sun, J., Singh, V., Kajino-Sakamoto, R., and Aballay, A. (2011). Neuronal GPCR controls innate immunity by regulating noncanonical unfolded protein response genes. Science *332*, 729–732.

Sun, X., Chen, W.D., and Wang, Y.D. (2017). DAF-16/FOXO transcription factor in aging and longevity. Front. Pharmacol. *8*, 548.

Troemel, E.R., Chou, J.H., Dwyer, N.D., Colbert, H.A., and Bargmann, C.I. (1995). Divergent seven transmembrane receptors are candidate chemosensory receptors in *C. elegans*. Cell *83*, 207–218.

Troemel, E.R., Chu, S.W., Reinke, V., Lee, S.S., Ausubel, F.M., and Kim, D.H. (2006). p38 MAPK regulates expression of immune response genes and contributes to longevity in C. elegans. PLoS Genet. *2*, e183.

Wu, Q., Cao, X., Yan, D., Wang, D., and Aballay, A. (2015). Genetic screen reveals link between the maternal effect sterile gene mes-1 and pseudomonas aeruginosa-induced neurodegeneration in *Caenorhabditis elegans*. J. Biol. Chem. *290*, 29231–29239.

Yatsunenko, T., Rey, F.E., Manary, M.J., Trehan, I., Dominguez-Bello, M.G., Contreras, M., Magris, M., Hidalgo, G., Baldassano, R.N., Anokhin, A.P., et al. (2012). Human gut microbiome viewed across age and geography. Nature *486*, 222–227.

STAR★METHODS

KEY RESOURCES TABLE

REAGENT or RESOURCE	SOURCE	IDENTIFIER
Bacterial and Virus Strains		
Escherichia coli OP50	Caenorhabditis Genetics Center	Wormbase ID: OP50
Pseudomonas aeruginosa PA14	Laboratory of Frederick M. Ausubel	PA14
Ahringer RNAi Libraries in *E. coli* HT115 (DE3)	Source BioScience	N/A
Enterococcus faecalis OGIRF	Laboratory of Danielle A Garsin	OGIRF
Chemicals, Peptides, and Recombinant Proteins		
Ethyl-methanesulfonate (EMS)	Millipore Sigma	Catalog No. M0880
Isopropyl-β-D-thiogalactoside	Anatrace	Catalog No. I1003
Proteinase K	QIAGEN	Catalog No. 19131
KpnI Restriction enzyme	NEW ENGLAND Biolabs	Catalog No. R0142S
SalI-HF Restriction enzyme	NEW ENGLAND Biolabs	Catalog No. R3138S
SphI-HF Restriction enzyme	NEW ENGLAND Biolabs	Catalog No. R3182S
BamHI Restriction enzyme	NEW ENGLAND Biolabs	Catalog No. R3136S
T4 DNA Ligase	NEW ENGLAND Biolabs	Catalog No. M0202S
Phusion High -Fidelity PCR Kit	NEW ENGLAND Biolabs	Catalog No. M0531S
Dream Taq Green PCR Master Mix (2X)	Thermo Fisher Scientific	Catalog No. K1081
Critical Commercial Assays		
Gentra Puregene kit	QIAGEN	Catalog No. 158667
RNeasy Plus Universal Kit	QIAGEN	Catalog No. 73404
TURBO DNase	Life Technologies	Catalog No. AM1907
High-Capacity cDNA Reverse Transcription Kit	Applied Biosystems	Catalog No. 4368814
Power SYBR PCR Master Mix	Applied Biosystems	Catalog No. 4367659
Deposited Data		
Raw and analyzed mRNA-Seq data	This study	GEO: GSE137112
Experimental Models: Organisms/Strains		
N2 *C.elegans* wild isolate	*Caenorhabditis* Genetics Center	WormBase ID: N2
unc-86::myr GFP + *odr-1*::RFP	*Caenorhabditis* Genetics Center	Strain CX5974
F49H12.4::GFP + unc-119(+)	*Caenorhabditis* Genetics Center	Strain NC1686
fer-1(b232ts)	*Caenorhabditis* Genetics Center	Strain HH142
kyIs104	*Caenorhabditis* Genetics Center	Strain CX3553
daf-16 (mu86)	*Caenorhabditis* Genetics Center	Strain CF1038
daf-16p::daf-16a/b::GFP + rol-6(su1006)	*Caenorhabditis* Genetics Center	Strain TJ356
unc-86::myr GFP + odr-1::RFP;F49H12.4::GFP + unc-119(+)	This study	N/A
srbc-48(ac23);F49H12.4::GFP + unc-119(+)	This study	N/A
unc-86::myr GFP + odr-1::RFP; daf-16p::daf-16a/b::GFP + rol-6(su1006)	This study	N/A
srbc-48(ac23); daf-16p::daf-16a/b::GFP + rol-6(su1006)	This study	N/A
odr-1p::srbc-48::GFP;daf-16p::daf-16a/b::GFP + rol-6(su1006)	This study	N/A
srbc-48p::srbc-48;daf-16p::daf-16a/b::GFP + rol-6(su1006)	This study	N/A
srbc-48(ac23);daf-16 (mu86)	This study	N/A

(*Continued on next page*)

Continued

REAGENT or RESOURCE	SOURCE	IDENTIFIER
Oligonucleotides		
See Table S6 for the primers used in the study	Integrated DNA Technologies	N/A
Recombinant DNA		
srbc-48p::srbc-48	This study	N/A
odr-1p::srbc-48::GFP	This study	N/A
odr-1p::RFP	This study	N/A
srbc-48p::GFP	This study	N/A
odr-1p::RFP; P*srbc-48*::GFP	This study	N/A
Software and Algorithms		
Prism7	Graph Pad Software, La Jolla, CA	https://www.graphpad.com/scientificsoftware/prism/
Snapgene	GSL Biotech	https://www.snapgene.com
ImageJ	NIH	https://imagej.nih.gov/ij/
Galaxy	N/A	https://usegalaxy.org
Database for Annotation, Visualization, and Integrated Discovery (DAVID)	N/A	https://david.ncifcrf.gov/

RESOURCE AVAILABILITY

Lead Contact

Further information and requests for resources and reagent should be directed to and will be fulfilled by the lead contact, Alejandro Aballay (aballay@ohsu.edu)

Materials Availability

All reagents generated in this study are available from the Lead contact without restriction.

Data and Code Availability

The accession number for the RNA seq data reported in this paper is Gene Expression Omnibus (GEO: GSE137112).

EXPERIMENTAL MODEL AND SUBJECT DETAILS

The *C. elegans* strains used in the study wild-type N2 Bristol, CX5974 (*kyIs262*), NC1686 (*wdIs51*), HH142 [*fer-1(b232ts)*], CF1038 [*daf-16(mu86)*], CX3553 (*kyIs104*) and TJ356 *(zIs356)* were procured from the *Caenorhabditis* Genetics Center (University of Minnesota, Minneapolis, MN). The following lines were constructed using standard genetic manipulation techniques: AY145[P*srbc-48::srbc-48*], AY146[P*odr-1p::srbc-48::*GFP], AY147[*odr-1::*RFP], AY148[P*srbc-48p*::GFP], AY149[*odr-1::RFP;* P*srbc-48p::*GFP], AY151 [AY-23; wdIs51], AY152[kyIs262; mu86], AY153 [AY-23; mu86], AY154 [kyIs262; *zIs356*], and AY155 [AY-23; *zIs356*]. The rescue strain AY145 was constructed by injecting P*srbc-48*::*srbc-48* and co-injecting the marker *Punc-122*::GFP into *srbc-48(ac23)* animals. All strains were cultured on plates containing nematode growth medium (NGM) and maintained at 20°C. *fer-1* animals were grown at the 15°C permissive temperature. All experiments were performed using hermaphrodites at young adult stage.

The bacterial strains used were *Escherichia coli* OP50, *E. coli* HT115 (DE3), *Enterococcus faecalis* (OG1RF), and *Pseudomonas aeruginosa* PA14. The cultures for these bacteria were grown in Luria-Bertani (LB) broth overnight at 37°C. *E. faecalis* was grown in brain-heart infusion (BHI) broth.

METHOD DETAILS

Forward Genetic Screen for Mutants Susceptible to Pathogen-Mediated Dendrite Degeneration

Ethyl-methanesulfonate (EMS) mutagenesis was performed using the CX5974 strain, which expresses red fluorescent protein (RFP) in AWC and AWB neurons. Approximately 3,000 synchronized late L4 larvae of CX5974 were treated with 50mM EMS for 4h followed by washing with M9 buffer three times for 2 hours. The washed animals (P0 generation) were then transferred to large Petri dishes (10 cm) containing *E. coli* OP50, and these animals were allowed to lay eggs (F1 progeny) overnight. The animals corresponding to the P0 generation were then washed away with M9 buffer, and the F1 eggs that remained attached to the plates were allowed to grow

until adulthood. After one day, the F1s and any hatched F2 progeny were removed by washing. The eggs of the F2s, which remained attached to the plates after washing, were allowed to develop to young adults on *E. coli* OP50. These animals were observed under a fluorescent microscope and mutants exhibiting any morphological changes in the dendrites were removed. The remaining mutants were transferred to plates containing PA14 and incubated for 24 hours at 25°C. The animals that showed any morphological changes in dendrites at 24 hours were transferred to individual plates. Approximately 80,000 haploid genomes were screened. Animals showing above 65% phenotype were backcrossed six times to the parental CX5974 strain before further analysis.

Fluorescence Imaging

Confocal fluorescent images of AWC, AWB and PVD neurons were taken with a Zeiss confocal microscope system (LSM-780) and Apotome Zeiss microscope with grid-based optical sectioning using a 20X and 40X objective water-immersion lens. Animals were immobilized with 20 mM sodium-azide in M9 buffer, mounted on a 2% agar pad, and covered with a glass coverslip. The screening of the mutants was done using a Leica M165 FC fluorescence microscope.

Quantification of Dendrite Degeneration

Animals were visualized for morphological changes in the dendrites, which are considered as hallmarks of neurodegeneration, including soma branching, wavy dendrites, dendrite branching, and beaded dendrites. Animals exhibiting the aforementioned morphological changes were considered as having dendrite degeneration. Briefly, the bacterial lawns used for the degeneration assay were prepared by spreading 300ul of the 8-10 hours culture of *P. aeruginosa* and *E. faecalis* over the entire surface of modified NGM or BHI agar media, respectively, in 6-cm diameter plates and incubated at 37°C. Young adult nematodes were transferred to *P. aeruginosa* or *E. faecalis* plates and grown for 24 hours at 25°C (Wu et al., 2015). For microscopy, the animals were anesthetized using 20 mM sodium-azide in M9 buffer, mounted onto agar pads, and visualized using a Zeiss microscope or Leica M165 FC microscope.

This assay was done five times with 50 *srbc-48(ac23)* and control animals. The percentage of the animals exhibiting dendrite degeneration phenotypes was calculated by dividing the number of animals showing dendrite degeneration by the total number of animals in each group. To analyze PVD and AWB dendrite degeneration, the animals expressing GFP in the PVD and AWB neurons were crossed to control and *srbc-48(ac23)* animals and then checked for the dendrite degeneration phenotypes after 24 hours of *P. aeruginosa* and *E. faecalis* infection. Animals displaying bead dendrites, broken dendrites, or bubble-like structures were scored as exhibiting dendrite degeneration. Animals were only considered exhibiting the dendrite degeneration phenotype if the number of beads was more than 3-4 or along the whole length of the dendrite (Oren-suissa et al., 2010). The number of animals observed in each group was 20 and the magnification used was 40X and was repeated three times.

Whole-Genome Sequencing and Data Analysis

For whole-genome sequencing, the DNA of the mutant animals was extracted. Briefly, the mutants were grown at 20°C on 10 cm NGM plates seeded with *E. coli* OP50. These animals were grown until starvation, and then the plates were rinsed thrice with M9 buffer to remove any bacteria. Then, the animals were incubated in M9 buffer with rotation for 2h and washed three times with M9 buffer to remove bacteria from the intestine. The genomic DNA was extracted using the Gentra Puregene kit (QIAGEN, Netherlands). The DNA was subjected to whole-genome sequencing (WGS) on an Illumina HiSeq 4000 sequencing platform using 50 single-end nucleotide reads, and DNA libraries were prepared according to a standard Illumina (San Diego, CA) protocol. Library preparation and WGS were performed at Novogene Genomic Services & Solutions Company, USA.

For analyzing the whole-genome sequence data, the EMS density mapping workflow from the Cloud Map program of the Galaxy web platform was used (Minevich et al., 2012). A list of single nucleotide polymorphisms (SNPs) in the mutant was generated by comparing it with the reference *C. elegans* (WS220). After that, the common SNPs were subtracted, and linkage maps for the mutants were created.

C. elegans Killing Assay on *P. aeruginosa* and *E. faecalis*

Synchronized animals were obtained by allowing gravid animals to lay eggs on NGM plates for 4-6 hours at 20°C. The bacterial lawns used for *C. elegans* killing assays were prepared by spreading 300 ul of 8-10 hours grown culture of *P. aeruginosa* and *E. faecalis* on the complete surface of modified NGM agar medium (0.35% peptone) and BHI (brain heart infusion) agar media, respectively. The plates were subsequently incubated overnight at 37°C and then cooled to room temperature for at least 1 hour before seeding them with synchronized young adult animals. The killing assays were performed at 25°C, and live animals were transferred daily to fresh pathogen seeded plates. Animals were scored at the indicated times and were considered dead when they failed to respond to the touch of a platinum wire. Each experiment was done in triplicate with 20 worms in each group.

Osmotic Stress Assay

The plates were prepared by adding 29.22 g/L of NaCl instead of 3.0 g/L into the NGM plates as previously described (Solomon et al., 2004). Synchronized 30 young adult animals were washed with the M9 buffer thrice to remove any bacteria. Then, the pellet of the

worms was added into the center of a 500 mM NaCl plate seeded with *E. coli*. Mutant and control animals were observed after 12 hours of exposure to check for any morphological changes in their dendrites. Each experiment was done with 20 worms in each group and repeated three times.

Cold tolerance Assay

Synchronized young adult animals were added on standard NGM plates seeded with OP50 bacteria. These plates were then transferred to a 4°C for 24 hours as previously described (Ohta et al., 2014). After 24 hours, the plates were stored at 20°C for 4 hours to allow the animals to recover from the cold stress. Then the animals were scored for changes in their dendrites. The experiment was repeated three times with 20 worms in each group.

C. elegans Longevity Assay

Lifespan assays were performed without uninfected animals and animals infected with *P. aeruginosa* infection for 8, 12, and 24 hours at 25°C. After infection, mutant or control animals grown on *P. aeruginosa* were rinsed by transferring them into 100 μL M9 containing 300 μg/ml concentration of streptomycin on NGM plates seeded with *E. coli* OP50. To remove any bacteria attached to the body wall, the animals were allowed to crawl out of the solution toward the OP50 lawn. Animals were further transferred onto new plates containing dead *E. coli* OP50 prepared by concentrating the overnight cultures at a 1:20 ratio and heat-killed at 100°C for 60 min. These plates were also supplemented with streptomycin (100 μg/ml), kanamycin (50 μg/ml) and Nystatin (10 μg/ml) to avoid contamination. A 350 μL drop of the killed bacteria was plated on a 6-cm plate and incubated at 25°C. Animals were scored at the indicated times for survival, and live animals were transferred to fresh plates if needed. Each experiment was repeated three times with 50 worms in each group and triplicate sets. For the lifespan assay after RNAi, second generation RNAi worms were used. These RNAi animals were exposed to PA14 for 24 hours at 25°C and analyzed as described above. This experiment was repeated twice with 50 worms in each group and duplicate sets.

Cloning and Generation of Transgenic *C. elegans* Strains

For *srbc-48* rescue, plasmid pSK1(pPD95.77_P*srbc-48::srbc-48*) was constructed by cloning gene *srbc-48* with its 4kb promoter into the KpnI and SmaI sites of the pPD95.77 vector (Fire Lab *C. elegans* Vector Kit; Addgene, Cambridge, MA). To prevent gene products to fuse with GFP, plasmid pRK1 (pPD95.77_SL2::GFP) was used (Cao et al., 2017). For the AWC-specific *srbc-48* rescue, plasmid pSK2 (pRK1_pPD95.77_P*odr-1*::*srbc-48*_SL2::GFP) were constructed by inserting 4kb of the *odr-1* promoter sequence upstream into the *SphI* and SalI sites and 1101bp of the *srbc-48* sequence into the SalI and BamHI sites of the plasmid pRK1. To identify the foci of *srbc-48* expression, plasmid pSK4 was constructed by cloning the 4kb promoter of *srbc-48* upstream into the KpnI and SmaI of the pRK1 vector. Transgenic strains were created by injecting 25 ng/μl of the plasmids together with 50 ng/μl of the co-injection marker P*unc-122*::GFP.

RNA Interference (RNAi)

RNA Interference was used for generating loss-of-function phenotypes by feeding worms *E. coli* strain HT115(DE3) expressing double-stranded RNA (dsRNA) homologous to a target gene. *E. coli* with the appropriate vectors were grown overnight at 37°C in LB broth containing ampicillin (100 μg/ml). The bacteria were then plated onto RNAi plates, which were NGM plates containing ampicillin (100 μg/ml) and 3 mM isopropyl β-D-thiogalactoside (IPTG). RNAi-expressing bacterial clones were allowed to grow overnight at 37°C. Gravid adults were transferred to RNAi-expressing bacterial lawns and allowed to lay eggs for 2 hours. The gravid adults were removed, and the eggs were allowed to develop at 20°C for 2 days. Gravid adults were then transferred to fresh RNAi-expressing bacterial lawns and allowed to lay eggs for 2 hours to synchronize a second-generation RNAi population. The gravid adults were removed, and the eggs were allowed to develop at 20°C to reach the young adult stage for experimental use. In all experiments, *unc-22* RNAi was included as a positive control to account for the RNAi efficiency.

Assay for DAF-16 Nuclear Localization

After 24 hours of pathogen infection, mutant and control animals were washed with M-9 buffer followed by washing with the antibiotic streptomycin and transferred to plates seeded with heat-killed OP50. The animals were mounted in M9 onto microscope slides after 24 hours, 5 days, and 10 days. The slides were viewed using a Zeiss fluorescence microscope. The DAF-16 localization was studied as cytosolic, nuclear and intermediate localization as described (Oh et al., 2005). This assay was done in triplicate with 20 animals in each group.

Chemotaxis Assay

The assay for odor chemotaxis was performed as previously described (Leinwand et al., 2015) to check the function of the AWC neurons. AWC olfactory neurons play an important role in chemotaxis to volatile odorants like isoamyl alcohol, 2, 3 pentanedione, 2, 4,5 trimethylthiazole, benzaldehyde, and butanone. Briefly, synchronized young adult nematodes were transferred to plates seeded with *P. aeruginosa* for 24 hours at 25°C. After the incubation, the animals were washed three times with S basal buffer to remove any bacteria, suspended in a smaller volume of S basal, and added onto the center of the chemotaxis plate. Washed animals were placed on the plate and allowed to move freely for one hour. Then, 1ul of sodium azide was added to the odor spots to anesthetize animals

reaching the end points. The underside of a chemotaxis plate was divided into 4 equal quadrants and a circle of 0.5 cm around the origin of the plate. Each quadrant was marked with either "BZ" for "Benzaldehyde"(0.2% vol/vol, in ethanol) or "Ctrl" for "95% Ethanol" and marks were equidistant from the center and each other. Five assays were performed in triplicates and on different days. The chemotaxis index was computed as the number of animals in the odor region minus the number of animals in the control region. The chemotactic index (CI) was calculated by the equation below:

$$\text{Chemotactic Index } (CI) = \frac{(\#\text{ worms at BZ}) - (\#\text{ worms at Ctrl})}{\#\ worms\ total}$$

RNA Isolation and Quantitative Real-Time PCR

Synchronized animals were placed on NGM plates seeded with *E. coli* OP50 and grown at 20°C until the animals reached the young adult stage. Animals were collected and washed with M9 buffer three times to remove any bacteria and then were transferred to modified NGM plates containing *E. coli* OP50 or *P. aeruginosa* PA14 for 24 hours at 25°C. The *P. aeruginosa* plates were prepared by spreading the 300 μl of *P. aeruginosa* culture on the modified NGM plates and then incubated overnight at 37°C. These animals were then washed off the plates with M9 buffer 3-4 times and frozen in TRIzol (Life Technologies, Carlsbad, CA). Total RNA extraction was done using the RNeasy Plus Universal Kit (QIAGEN, Netherlands). Residual genomic DNA was removed using TURBO DNase (Life Technologies, Carlsbad, CA). A total of 2 μg of total RNA was reverse transcribed with random primers using the High-Capacity cDNA Reverse Transcription Kit (Applied Biosystems, Foster City, CA). Quantitative RT-PCR was conducted using Power SYBR PCR Master Mix (Applied Biosystems, Foster City, CA) on an Applied Biosystems 7900HT real-time PCR machine in 96-well plate format using 25 μL in each reaction. The relative fold-changes of the transcripts were calculated using the comparative C_T ($2^{-\Delta\Delta CT}$) method and normalized to pan-actin values obtained by using the Step-OnePlus Software (Life Technologies, Carlsbad, CA). Three technical replicates of samples were used, and the experiment was repeated three times.

RNA Sequencing and Gene Expression Analysis

RNA Sequencing (RNA-Seq) was done for gene-expression analysis and transcriptomic studies. The total RNA of *fer-1*(b232ts) and *srbc-48(ac23)*; *fer-1*(b232ts) animals was isolated from three biological replicates as described above. The sample integrity and purity were checked using Agilent 2100. The RNA was sequenced on HiseqX sequencing platform-using 150bp paired-end nucleotide reads. The RNA sequencing libraries were prepared using a NEBNext® Ultra RNA Library Prep Kit for Illumina® (NEB#E7530L). Library preparation and sequencing were performed at the Novogene Genomic Services & Solutions Company, USA.

The RNA sequence data was analyzed using the Galaxy. The sequenced reads obtained for each sample were mapped to the *C. elegans* genome (WS255) using the aligner STAR. For sequencing depth, an RNA composition counts were normalized across all samples. Differential gene expression analysis was then performed on normalized samples using DESeq2. Genes exhibiting at least two-fold change and a false-discovery rate (FDR) of 0.05 were considered differentially expressed. Analysis for gene enrichment, gene ontology (GO), or biological processes was performed using the Database for Annotation, Visualization, and Integrated Discovery (DAVID) (https://david.ncifcrf.gov/). The overlap of the upregulated genes in previously studied pathways, including DAF-16, PMK-1, CEP-1/p53 and SKN-1 regulated genes (Derry et al., 2007; Murphy et al., 2003; Oliveira et al., 2009; Troemel et al., 2006), was calculated. Statistical significance of the overlap between two gene sets was calculated using the following on-line program: nemates.org/MA/progs/overlap_stats.html. Representation Factor represents the number of overlapping genes divided by the expected number of overlapping genes drawn from 2 independent groups.

QUANTIFICATION AND STATISTICAL ANALYSIS

Statistical analysis was performed using Graph Pad Prism 8 (Graph Pad Software, La Jolla, CA). Survival curves were considered statistically significant when p values were < 0.05. The Kaplan-Meier method was used to calculate the survival fractions, and statistical significance between survival curves was determined using the log-rank test. Dendrite degeneration was studied in groups of 20 animals and the results are shown as mean ± SEM, treating each experiment as one data point. Significance was calculated by two-sample t test, and assuming a normal distribution. Data normality was confirmed using the D'Agostino-Pearson and Shapiro-Wilk tests. Each experiment was repeated at least three times and each comparison was done with the corresponding control group individually. In figures, all bars represent mean ± SEM and asterisks (*) denote p value as *$p < 0.05$, **$p < 0.01$, ***$p < 0.001$, ****$p < 0.0001$, NS, not significant.